Interactions Between Fluids and Elastic Solids Math+ 2024

Zachary Robers, Michael Thomas, Olly Yang

February 3, 2025

1 Abstract

We study a simplified model of a one-dimensional fluid-structure interaction problem consisting of nonlinear shallow water waves coupled to a linearized elasticity model with the boundary between the fluid and solid domains allowed to freely move. In order to couple the fluid and solid problems together and describe the motion of the interface, we turn to physical principles such as mass and energy conservation in order to provide the necessary coupling conditions. Our analysis of the system consists of a two-pronged approach of linear stability analysis and numerics. In our linear stability analysis, we follow the approach of Lax and Majda's work on the stability of shocks to analyze the stability of the associated linearized problem. MacCormack's method for finite difference serves as the basis of our numerical model. This classical numerical method achieves quadratic convergence for either the shallow water equation or linear wave equation in isolation. We then combine these equations along the moving boundary using a scheme rooted in energy conservation to study the behavior of the full coupled system with a moving boundary. Our analysis provides a first step towards studying important physical applications such as the iceberg calving problem. In our simplified setting, we are able to simulate the dynamics of an incoming fluid swell by using suitably chosen boundary conditions on the left side of the computational window.

2 Introduction

The study of fluid-structure interactions (FSI), while typically performed numerically with the Navier-Stokes Equations, remains a field rich in theoretical and practical implications in extension to the interactions of shallow water waves and elastic solids. This paper aims to explore the dynamics of such interactions by focusing on a simplified model that couples nonlinear shallow water waves with a linearized elasticity model, with a free-

moving boundary between the fluid and solid domains.

$$\begin{aligned} \frac{\partial \zeta}{\partial t} + \frac{\partial}{\partial x}(hv_f) &= 0, \qquad x < X(t), \\ \frac{\partial v_f}{\partial t} + v_f \frac{\partial v_f}{\partial x} + g\frac{\partial \zeta}{\partial x} &= 0, \qquad x < X(t), \\ \frac{\partial w}{\partial t} - \frac{\partial v_s}{\partial x} &= 0, \qquad x > X(t), \\ \frac{\partial v_s}{\partial t} - \frac{\partial}{\partial x}(\frac{E}{\rho_s} w) &= 0, \qquad x > X(t), \end{aligned} \tag{2.1}$$

where ζ is the deviation from equilibrium fluid depth, h is the total fluid depth, v_f is the fluid velocity, $w = \frac{\partial u}{\partial x}$ is the solid deformation, $v_s = \frac{\partial u}{\partial t}$ is the solid velocity, E is the elastic modulus of the solid, and ρ_s is the solid density. In section 3, we derive kinematic and energy boundary conditions and the ODE for the interface between the fluid and solid to complete this model (see 3.7 for the complete theorem).

This model is in part motivated as an attempt to simulate real-world phenomena such as iceberg calving, where fluid forces impact the dynamics of a glacier, causing an iceberg to break off. Our model has several simplifications from its geophysical motivation, namely the domain extends infinitely away from the moving boundary between the fluid and solid and the solid extends to the seafloor, which is different compared to geophysical problem where we would expect ice to be floating above some water. While these simplifications make it difficult to directly apply our model to the iceberg calving phenomenon which is more analogous to shock formation in this more complex domain, the study of how this simplified system at equilibrium responds to perturbations is a towards elucidating the dynamics which could lead to an iceberg calving event.

Métivier among others [2, 4, 5, 7, 8, 9, 10] have made numerous contributions to the field of shock dynamics, relevant to the well-posedness of our work as the fluid-solid interface can be viewed as a de facto mathematical shock in the system even though the boundary itself is not a physical shock wave. These works are mainly concerned with shocks in traditional systems of conservation laws where the flux is the same on both sides. Lax's early works in 1957 provide insights on identification of physical 1D shocks and how they relate to entropy conditions for scalar equations and determining which piecewise constant states could exist physically [4]. This was further refined by Majda's work, which extended Lax's argument to multiple dimensions and obtained a short time existence result for perturbations of shocks [7, 8, 9]. Métivier's 2001 study offered a subtle refinement of Majda's results, in addition to the discussion on the stability of multidimensional shocks [10]. In our problem, the moving interface, viewed as a shock, introduces discontinuities to the system at the fluid-solid boundary. For this reason, the combined works referenced above give us a foundation to study the coupled problem.

Earlier studies on wave propagation in elastic solids, as summarized by Achenbach, highlight key considerations for modeling the deformation of elastic materials [1]. In his compilation, Achenbach emphasizes that referencing an undeformed resting state—one to which the solid naturally returns in the absence of external forces—is a more intuitive approach, thereby supporting the adoption of the material (Lagrangian) description for modeling elasticity. Given that fluids typically are modeled in the Eulerian coordinate system as it makes sense to track the movement of a particle in space without reference to a undeformed state, within our FSI model, we initially represent the shallow water equations in the Eulerian coordinate system and the elastic wave equation in the Lagrangian

coordinate system. Ergo, a key component in the derivation of our kinematic and energy boundary conditions is the unification of the model under the Eulerian coordinate system.

The nonlinear shallow water wave equations, also known as the Saint-Venant equations, are a common choice for modeling fluid dynamics in shallow water contexts as they follow from Euler's equations when the horizontal scale is much greater than the vertical scale. See [3] and sources therein for justification of the Saint-Venant equations. Furthermore, in partnership with Tatsuo Iguchi, Lannes' 2021 paper provided a theorem for the existence of hyperbolic free boundary problems like the model established in (2.1), subject to boundary conditions derived in section 3 [2]. In order to apply said existence theorem, we must linearize the boundary conditions derived in 3 in the coupled shallow water and elastic solid system. After this linearization, our model then satisfies Iguchi and Lannes' linear boundary conditions presented in Section 3.1, enabling us to directly cite their theorem for proof of existence.

The first part of this work focuses on establishing the coupled model such that conservation of mass and energy are satisfied. The resulting conditions and an ordinary differential equation (ODE) governing the location of the moving boundary together with the fluid and solid equations comprise the complete model for the FSI problem we seek to study. From here, we turn to Iguchi and Lannes' work in our discussion of well-posedness to prove the existence of solutions to our model. Then, we take the two pronged approach of linear stability analysis and numerical simulation to analyze how the model responds to a disruption from equilibrium. The linear stability analysis follows the work of Lax, Majda, and Métivier to understand the affect of the interface de facto mathematical shock on the model [10, 7, 8, 9].

MacCormack's method for finite difference, along with a second-order scheme to approximate the location of the moving boundary and reconcile domain shifts between the fluid and solid domains, is the basis of the deployed numerical approach [6]. Encompassing a periodic forcing through a fictitious boundary condition on the fluid domain aligns the numerical approach with geophysical motivation by modeling a discrete response of the elastic solid to a fluid force.

This work lends way to several open problems which, if resolved, would allow our model to better align with the geophysical motivation of iceberg calving. One such problem is our assumption that the iceberg extends to the seafloor: an assumption we make so that we can assume uniform atmospheric pressure above the fluid, which plays a crucial rule in deriving the second equation in (2.1). An additional vertical spatial dimension could enable a model to include the vertical component of the fluid velocity vector field so that we could model the more complex dynamics of deep water. The dynamics of the open ocean around a glacier can also be modeled by a fluid model which includes a viscous term, such as a more complex version of the Saint-Venant Equations. Furthermore, more sophisticated models of elasticity would make possible the examination of the stress-strain relationship and domain fracturing, leading to greater understanding of the conditions which cause an iceberg to break from a glacier. From here, the solid model can be further adjusted to better match the shape of a real-world iceberg and encompass a non-uniform material composition.

3 Modeling

As outlined in the introduction, our one-dimensional coupled system consists of fluid on one side, an elastic solid on the other side, and a moving boundary in between the fluid and solid components. The fluid side is arbitrarily positioned on the left of our model. Accordingly, the elastic solid is positioned on the right. We define $X(t)$ to be the location of the moving fluid-solid boundary. Note that the fluid on the left is without loss of generality, reflecting through $X(t)$ swaps left and right. Since we are primarily interested in investigating the behavior of the system local to the moving boundary, both the fluid and solid domains extend infinitely in the direction opposite of the moving boundary. This enables us to make key simplifications and avoid additional boundary considerations.

Remark 3.1. *Even though periodic boundary conditions generically eliminate additional boundary considerations and have some major technical aspects which make them easier to work with, they are not possible here as they would create secondary moving boundaries, which would significantly complicate the problem.*

We model the fluid using the the nonlinear shallow water wave (Saint-Venant) equations

$$\begin{aligned} \frac{\partial \zeta}{\partial t} + \frac{\partial}{\partial x}(h v_f) &= 0, \qquad && x < X(t), \\ \frac{\partial v_f}{\partial t} + v_f \frac{\partial v_f}{\partial x} + g\frac{\partial \zeta}{\partial x} &= 0, && x < X(t), \end{aligned} \tag{3.1}$$

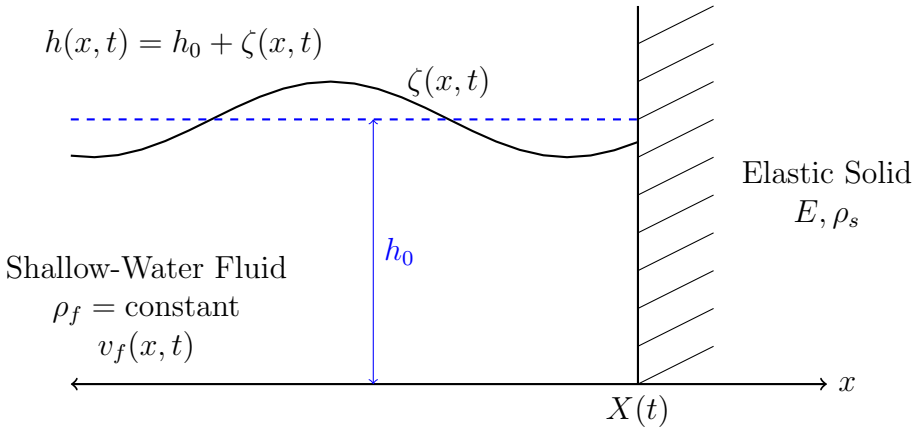

where ζ is the deviation from equilibrium fluid depth, $h = h_0 + \zeta$ is the total fluid depth, and v_f is the fluid velocity. We model the elastic solid on the right-hand side of the moving boundary using the standard linear wave equation, written as a first-order system

$$\begin{aligned} \frac{\partial w}{\partial t} - \frac{\partial v_s}{\partial x} &= 0, \qquad && x > X(t), \\ \frac{\partial v_s}{\partial t} - \frac{\partial}{\partial x}\left(\frac{E}{\rho_s} w\right) &= 0, && x > X(t), \end{aligned} \tag{3.2}$$

where $w = \frac{\partial u}{\partial x}$ is the solid deformation, $v_s = \frac{\partial u}{\partial t}$ is the solid velocity, E is the elastic modulus of the solid, and ρ_s is the solid density. Note that $u(x,t)$ is the displacement in the horizontal direction in the traditional second order formulation of the linear wave equation.

With the basis for our model established, we now seek to derive an ODE governing the behavior of the fluid-solid boundary. More specifically, we aim to confirm that the velocity of the boundary, $X'(t)$, is equal to the velocity of the solid and fluid at the location of the boundary. To do so, we start with the conservation of fluid mass:

$$\frac{\partial m_f}{\partial t} = \frac{d}{dt}\int_{-\infty}^{X(t)} \rho_f(h_0+\zeta)\,dx = 0. \tag{3.3}$$

Applying the Reynolds transport theorem and substituting from (3.1), the above becomes

$$\begin{aligned}\frac{d}{dt}\int_{-\infty}^{X(t)} \rho_f(h_0+\zeta)\,dx &= \rho_f\int_{-\infty}^{X(t)} \frac{\partial \zeta}{\partial t}\,dx + \rho_f X'(t)(h_0+\zeta(X(t),t)),\\ &= \rho_f\int_{-\infty}^{X(t)} -\frac{\partial}{\partial x}(hv_f)\,dx + \rho_f X'(t)h(X(t),t),\\ &= -\rho_f h(X(t),t)(v_f(X(t),t)-X'(t)) = 0.\end{aligned}$$

From this result, we gain our first ODE for the moving boundary which serves as a kinematic boundary condition on v_f.

Proposition 3.2. *The velocity of the fluid at the location of the contact line is equal to the derivative of the contact line:*

$$X'(t) = v_f(X(t),t). \tag{3.4}$$

While the fluid equations are more commonly given in the Eulerian coordinate system as variables track changes in time along fixed spatial grid, the derivation for equations of solid motion rely on the notion of a displacement field, a distinctively Lagrangian formulation [1]. Thus, the solid side of our coupled system is modeled in the Lagrangian coordinate system. As a result, to derive the kinematic boundary condition on the solid side, first we convert the linear wave equation in the Lagrangian setting to the Eulerian coordinate system, which subsequently becomes nonlinear:

$$\frac{E}{1-w}\frac{\partial}{\partial x}\left(\frac{w}{1-w}\right) = \rho_s\left(\frac{\partial}{\partial t}\left(\frac{v_s}{1-w}\right) + \frac{1}{2}\frac{\partial}{\partial x}\left(\frac{v_s^2}{(1-w)^2}\right)\right). \tag{3.5}$$

The solid velocity, deformation, and density in the Eulerian setting can be written as

$$v_E = \frac{v_s}{1-w}, \qquad w_E = \frac{w}{1-w}, \qquad \rho_s^E = \rho_s(1-w), \tag{3.6}$$

and thus (3.5) can also be written as

$$\frac{E}{1-w}\frac{\partial w_E}{\partial x} = \rho_s\left(\frac{\partial v_E}{\partial t} + \frac{1}{2}\frac{\partial}{\partial x}(v_E)^2\right). \tag{3.7}$$

To avoid the complexities introduced by this nonlinear formula in the Eulerian coordinate system, we perform a secondary linearization on v_E and w_E:

$$v_E = \frac{v_s}{1-w} = v_s + v_s w + v_s w^2 + \cdots \approx v_s, \qquad w_E = \frac{w}{1-w} \approx w. \tag{3.8}$$

Remark 3.3. *Our adaptation from [2] and our numerics can handle* (3.7) *with relatively minor adaptations if we break it into mass & momentum conservation;* (3.8) *was done solely for simplicity sake.*

Substituting (3.8) into (3.7) and simplifying yields the second equation from the linear wave equation system (3.2), now expressed in the Eulerian coordinate system thanks to a secondary linearization about $v_E = w_E = 0$. As for the other equation in (3.2), it can be obtained from the conservation of solid mass in the Eulerian setting

$$\frac{\partial \rho_s^E}{\partial t} + \frac{\partial}{\partial x}(\rho_s^E v_E) = 0, \tag{3.9}$$

with necessary substitutions from (3.6). As a result of following this process, we are back to the setting of the linear wave equation to model our solid in the Eulerian system. Furthermore, the linearization proposed in (3.8) enables us to disregard the deformation term in the denominator of (3.22) to yield the following kinematic boundary condition on the solid domain.

Proposition 3.4. *After imposing a secondary linearization on the velocity and deformation of the solid in Eulerian coordinates, the velocity of the solid at the boundary location equals the velocity of the contact line:*

$$X'(t) = v_s(X(t), t). \tag{3.10}$$

From here, we can combine this result with (3.4) to obtain our complete kinematic boundary condition which enforces continuity of velocity between the fluid and linearized solid domains.

Proposition 3.5. *The velocity of the fluid at the contact line equals the velocity of the solid at the contact line when the linear wave equation in Eulerian coordinates in linearized. That is, under this condition:*

$$v_f(X(t), t) = v_s(X(t), t). \tag{3.11}$$

Next, we seek to derive our second boundary condition using the global conservation of energy in our coupling system. Let $\mathcal{E}$ represent the total energy of the system, and then the conservation of energy is given by the following equation

$$\frac{d\mathcal{E}}{dt} = \frac{d}{dt}\left(\int_{-\infty}^{X(t)} e_f \, dx + \int_{X(t)}^{\infty} \hat{e}_s^E \, dx\right) = 0. \tag{3.12}$$

Note that

$$e_f = \frac{1}{2}\rho_f h v_f^2 + \frac{1}{2}\rho_f g \zeta^2, \tag{3.13}$$

is the fluid energy density satisfying local conservation of energy in Eulerian coordinates

$$\frac{\partial e_f}{\partial t} + \frac{\partial \mathcal{F}_f}{\partial x} = 0, \tag{3.14}$$

where $\mathcal{F}_f$ is the fluid energy flux density given by

$$\mathcal{F}_f = \Pi h v_f, \tag{3.15}$$

where $\Pi = \frac{1}{2}\rho_f {v_f}^2 + \rho_f g \zeta$ is the hydrodynamic pressure. However, the solid initially is in Lagrangian coordinate system, with local energy conservation in Lagrangian coordinates

$$\frac{\partial e_s}{\partial t} + \frac{\partial \mathcal{F}_s}{\partial x} = 0, \tag{3.16}$$

where e_s and $\mathcal{F}_s$ are the solid energy density and energy flux density in Lagrangian coordinates, and we'd like to have everything in the Eulerian setting. Hence, we seek the following conversion from Lagrangian to Eulerian coordinates

$$\frac{\partial e_s}{\partial t} \longrightarrow \frac{\partial e_s^E}{\partial t} + v_E \frac{\partial e_s^E}{\partial x}, \qquad \frac{\partial \mathcal{F}_s}{\partial x} \longrightarrow \frac{1}{1-w_s}\frac{\partial \mathcal{F}_s^E}{\partial x}, \tag{3.17}$$

where

$$e_s^E = \frac{1}{2}\rho_s {v_E}^2 + \frac{1}{2}E{w_E}^2, \qquad \mathcal{F}_s^E = -Ewv_E, \tag{3.18}$$

are the energy density and energy flux density in the Eulerian setting. Substituting these conservation rules (3.17) into (3.16) yields

$$\frac{\partial e_s^E}{\partial t} + v_E \frac{\partial e_s^E}{\partial x} + \frac{1}{1-w_s}\frac{\partial e_s^E}{\partial t} = 0. \tag{3.19}$$

We can rewrite the above as

$$\frac{\partial \hat{e}_s^E}{\partial t} + \frac{\partial \hat{\mathcal{F}}_s^E}{\partial x} = 0, \tag{3.20}$$

where $\hat{e}_s$ and $\hat{\mathcal{F}}_s$ are the updated solid energy density and energy flux density in the Eulerian setting given by

$$\hat{e}_s^E = (1-w_s)e_s^E, \qquad \hat{\mathcal{F}}_s^E = \mathcal{F}_s^E + v_s e_s^E. \tag{3.21}$$

Now that we have expressions for the energy and energy flux densities for the fluid and solid in the Eulerian system, we can proceed with deriving an energy coupling condition from global conservation of energy. Applying the Reynolds transport theorem to (3.12) and make appropriate substitutions from (3.14) and (3.20) yield

$$\begin{aligned}
\frac{d\mathcal{E}}{dt} &= \int_{-\infty}^{X(t)} \frac{\partial e_f}{\partial t}\,dx + X'(t)e_f(X(t),t) + \int_{X(t)}^{\infty} \frac{\partial \hat{e}_s^E}{\partial t}\,dx - X'(t)\hat{e}_s^E(X(t),t)),\\
&= \int_{-\infty}^{X(t)} -\frac{\partial \mathcal{F}_f}{\partial x}\,dx + \int_{X(t)}^{\infty} -\frac{\partial \hat{\mathcal{F}}_s^E}{\partial x}\,dx + X'(t)(e_f(X(t),t) - \hat{e}_s^E(X(t),t)),\\
&= \underbrace{-\mathcal{F}_f\big|_{x=X(t)} + X'(t)e_f(X(t),t)}_{\text{fluid part}} + \underbrace{\hat{\mathcal{F}}_s^E\big|_{x=X(t)} - X'(t)\hat{e}_s^E(X(t),t)}_{\text{solid part}}.
\end{aligned}$$

For the solid part, from (3.6) the velocity of the contact line becomes

$$X'(t) = \left.\frac{v_s}{1-w}\right|_{x=X(t)}, \tag{3.22}$$

and hence with substitutions from (3.22) and (3.21), we have

$$\begin{aligned}
\hat{\mathcal{F}}_s^E\big|_{x=X(t)} - X'(t)\hat{e}_s^E(X(t),t) &= (\mathcal{F}_s + v_s e_s^E - X'(t)(1-w_s)e_s^E)\big|_{x=X(t)},\\
&= (\mathcal{F}_s + v_s e_s^E - \frac{v_s}{1-w_s}(1-w_s)e_s^E)\big|_{x=X(t)} = \mathcal{F}_s\big|_{x=X(t)}.
\end{aligned}$$

We can now express the energy and energy flux densities using (3.13), (3.15), and (3.18) while substituting using the kinematic boundary condition (3.4) to yield

$$\begin{aligned}\frac{d\mathcal{E}}{dt} &= -\mathcal{F}_f\big|_{x=X(t)} + X'(t)e_f(X(t),t) + \mathcal{F}_s\big|_{x=X(t)},\\ &= \left(-(\frac{1}{2}\rho_f v_f^2 + \rho_f g\zeta)hv_f + v_f(\frac{1}{2}\rho_f h v_f^2 + \frac{1}{2}\rho_f g\zeta^2) - Ewv_s\right)\Big|_{x=X(t)},\\ &= \left(-\frac{1}{2}\rho_f g v_f(2h\zeta - \zeta^2) - Ewv_s\right)\Big|_{x=X(t)},\\ &= -X'(t)\left(\frac{1}{2}\rho_f g(h^2 - h_0^2) + Ew\right)\Big|_{x=X(t)} = 0.\end{aligned}$$

From here, as the mass & momentum conservation system in Eulerian coordinates is Galilean invariant, we obtain the final formulation of our energy boundary condition.

Proposition 3.6. *In order to obey global conservation of energy, the system must follow the ensuing condition on the moving boundary between the fluid and solid domains*

$$\frac{1}{2}\rho_f g(h(X(t),t)^2 - h_0^2) + Ew(X(t),t) = 0. \tag{3.23}$$

Now that we have developed conditions to satisfy the conservation of mass and energy, we have all the components to properly define a one-dimensional model which couples the shallow water wave and elastic solid equations along a moving boundary.

Theorem 3.7. *The coupled shallow water wave and elastic solid system can be modeled as the following system of PDEs*

$$\begin{aligned}\frac{\partial\zeta}{\partial t} + \frac{\partial}{\partial x}(hv_f) &= 0, \qquad x < X(t),\\ \frac{\partial v_f}{\partial t} + v_f\frac{\partial v_f}{\partial x} + g\frac{\partial\zeta}{\partial x} &= 0, \qquad x < X(t),\\ \frac{\partial w}{\partial t} - \frac{\partial v_s}{\partial x} &= 0, \qquad x > X(t),\\ \frac{\partial v_s}{\partial t} - \frac{\partial}{\partial x}(\frac{E}{\rho_s}w) &= 0, \qquad x > X(t),\end{aligned} \tag{3.24}$$

subject to kinematic and energy boundary conditions

$$\begin{aligned}v_f(X(t),t) - v_s(X(t),t) &= 0,\\ \frac{1}{2}\rho_f g(h(X(t),t)^2 - h_0^2) + Ew(X(t),t) &= 0,\end{aligned} \tag{3.25}$$

and complemented by the ODE for the interface

$$X'(t) = v_f(X(t),t). \tag{3.26}$$

4 Well-posedness

Now we would like to recall the framework introduced by Iguchi-Lannes. Let us consider the following general system of PDEs with linear boundary conditions

$$\begin{aligned}\frac{\partial\vec{u}_L}{\partial t} + A_L(\vec{u}_L)\frac{\partial\vec{u}_L}{\partial x} &= 0, \qquad x \in (-\infty, X(t)),\\ \frac{\partial\vec{u}_R}{\partial t} + A_R(\vec{u}_R)\frac{\partial\vec{u}_R}{\partial x} &= 0, \qquad x \in (X(t), \infty),\end{aligned} \tag{4.1}$$

where $\vec{u}_L$, $\vec{u}_R \in \mathbb{R}^2$ and $A_L(\vec{u}_L)$, $A_R(\vec{u}_R)$ are 2×2 coefficient matrices, with initial values and subject to linear boundary conditions

$$\begin{aligned} \vec{u}|_{t=0} &= \vec{u}^{\text{in}}(x), \qquad x \in \mathbb{R}^- \cup \mathbb{R}^+, \\ N_p^r \vec{u} - N_p^l \vec{u} &= g(t), \qquad x = X(t), \end{aligned} \tag{4.2}$$

where $\vec{u} = \begin{pmatrix} \vec{u}_L \\ \vec{u}_R \end{pmatrix} \in \mathbb{R}^4$and $N_p^{l,r}$ are two $p \times 4$ matrices where the value of p depends on the speed of the interface relative to the eigenvalues. In our scenario, we set $p = 2$ and $g(t) = 0$, though this is a specialized case from a general result. Furthermore, $X(t)$ is the position of the interface satisfying $X(0) = 0$ without loss of generality. Section 3.3 of [2] constructs a change of variables $\varphi(\cdot, t) : \mathbb{R} \to \mathbb{R}$ such that $\varphi(x, 0) = x$ and for any $t \in [0, T]$, we have

$$\begin{aligned} \varphi(0, t) &= X(t), \\ \varphi(\cdot, t) &: \mathbb{R}^- \to (-\infty, X(t)), \\ \varphi(\cdot, t) &: \mathbb{R}^+ \to (X(t), \infty), \end{aligned} \tag{4.3}$$

to "freeze" the boundary at $x = 0$. As a result, we can merge the two PDEs in (4.1) map $x \to -x$ on the fluid side, yielding

$$\frac{\partial \vec{u}}{\partial t} + A(\vec{u}, \partial\varphi)\frac{\partial \vec{u}}{\partial x} = 0, \qquad x \in (0, T) \times \mathbb{R}^+, \tag{4.4}$$

where $\partial\varphi = \begin{pmatrix} \partial_x \varphi \\ \partial_t \varphi \end{pmatrix}$, and

$$A(\vec{u}, \partial\varphi) = \begin{pmatrix} A_1(\vec{u}_L, \partial\varphi_L) & 0_{2\times 2} \\ 0_{2\times 2} & A_2(\vec{u}_R, \partial\varphi_R) \end{pmatrix},$$

is the 4×4 block diagonal matrix merged from the matrices in (4.1) and with separate change of variables given in (4.3), and φ_L, φ_R are the individual change of variables for the fluid and solid side, respectively. In addition, (4.1) is complemented by their ODE for the interface

$$X'(t) = \chi(\vec{u}|_{x=0}), \tag{4.5}$$

for some smooth function χ defined on a domain of $\mathbb{R}^2 \times \mathbb{R}^2$. Section 1.3 of [2] considers the solution space $\mathbb{W}^m(T)$ of hyperbolic systems in the space $(0, T) \times \mathbb{R}^+$ as

$$\mathbb{W}^m(T) = \bigcap_{j=0}^{m} C^j([0, T]; H^{m-j}(\mathbb{R}^+)), \tag{4.6}$$

where $H^{m-j}(\mathbb{R}^+)$ is the classical Sobolev space. With that in mind, Theorem 3.19 of [2] states the following:

Theorem 4.1. *Let $m \geq 2$ be an integer; if $\vec{u}^{in} \in H^m(\mathbb{R}^+)$ takes its values in $\tilde{\mathcal{K}}_0 \times \mathcal{K}_0$ with $\tilde{\mathcal{K}}_0 \subset \tilde{\mathcal{U}}$ and $\mathcal{K}_0 \subset \mathcal{U}$ compact and convex sets, if $\vec{u}^{in}(0) \in \mathcal{U}_I$, and if the data $\vec{u}^{in}$ satisfies the compatibility conditions up to order $m-1$, then there exists a unique solution $(\vec{u}, X(t))$ to systems in the form of (4.4) complemented by the ODE for the interface (4.5) subject to the linear boundary conditions in (4.2) if*

a) $A_{L,R} \in C^\infty(\mathcal{U})$ and $\chi \in C^\infty(\mathcal{U}_I)$;

b) for all $\vec{u} = (\vec{u}_L, \vec{u}_R)^T \in \mathcal{U}$*, the matrices* $A_L(\vec{u}_L)$ *and* $A_R(\vec{u}_R)$ *have eigenvalues* $\pm\lambda_L^{\pm}(\vec{u}_L)$ *and* $\pm\lambda_R^{\pm}(\vec{u}_R)$*, respectively, with* $\lambda_{L,R}^{\pm} > 0$*;*

c) for any $\vec{u} \in \mathcal{U}_I$*, the Lopatinsky matrix associated with the subsonic interface is invertible;*

d) for any $\vec{u} = (\vec{u}_L, \vec{u}_R)^T \in \mathcal{U}_I$*, there holds* $\lambda_L^{\pm}(\vec{u}_L) \mp \chi(\vec{u}) > 0$ *and* $\lambda_R^{\pm}(\vec{u}_R) \mp \chi(\vec{u}) > 0$*, i.e the interface remains subsonic.*

Our coupled systems with (3.1) and (3.2) are indeed in the form described in (4.4), which now we will show. Let us combine (3.1) and (3.2) into one system and write them in conservative form

$$\begin{cases} \dfrac{\partial}{\partial t}\begin{pmatrix}\zeta\\ v_f\end{pmatrix} + \dfrac{\partial}{\partial x}\begin{pmatrix} hv \\ \frac{1}{2}{v_f}^2 + g\zeta\end{pmatrix} = 0, & x < X(t), \\ \dfrac{\partial}{\partial t}\begin{pmatrix}w\\ v_s\end{pmatrix} + \dfrac{\partial}{\partial x}\begin{pmatrix} -v_s \\ -\frac{E}{\rho_s}w\end{pmatrix} = 0, & x > X(t), \end{cases} \tag{4.7}$$

where

$$\mathcal{F}_f(\zeta, v_f) = \begin{pmatrix} hv \\ \frac{1}{2}{v_f}^2 + g\zeta\end{pmatrix}, \qquad \mathcal{F}_s(w, v_s) = \begin{pmatrix} -v_s \\ -\frac{E}{\rho_s}w\end{pmatrix},$$

are the corresponding fluid and solid flux. Applying the chain rule gives us the matrix form

$$\begin{cases} \dfrac{\partial}{\partial t}\begin{pmatrix}\zeta\\ v_f\end{pmatrix} + \begin{pmatrix} v_f & h \\ g & v_f\end{pmatrix}\dfrac{\partial}{\partial x}\begin{pmatrix}\zeta\\ v_f\end{pmatrix} = 0, & x < X(t), \\ \dfrac{\partial}{\partial t}\begin{pmatrix}w\\ v_s\end{pmatrix} + \begin{pmatrix} 0 & -1 \\ -\frac{E}{\rho_s} & 0\end{pmatrix}\dfrac{\partial}{\partial x}\begin{pmatrix}w\\ v_s\end{pmatrix} = 0, & x > X(t), \end{cases} \tag{4.8}$$

where

$$D\mathcal{F}_f = \begin{pmatrix} v_f & h \\ g & v_f\end{pmatrix}, \qquad D\mathcal{F}_s = \begin{pmatrix} 0 & -1 \\ -\frac{E}{\rho_s} & 0\end{pmatrix}.$$

Letting $\vec{u} = \begin{pmatrix}\zeta\\ v_f\\ w\\ v_s\end{pmatrix}$ and $A(\vec{u}, \partial\varphi)$ be the corresponding 4×4 block diagonal matrix made from the matrices in (4.8) yields our coupled system in the form of (4.4).

Theorem 4.2. *Let* $m \geq 2$ *be an integer; if* $\vec{u}^{in} \in H^m(\mathbb{R}^+)$ *takes its values in* $\tilde{\mathcal{K}}_0 \times \mathcal{K}_0$ *with* $\tilde{\mathcal{K}}_0 \subset \tilde{\mathcal{U}}$ *and* $\mathcal{K}_0 \subset \mathcal{U}$ *compact and convex sets, if* $\vec{u}^{in}(0) \in \mathcal{U}_I$*, and if the data* $\vec{u}^{in}$ *satisfies the compatibility conditions up to order* $m-1$*, then there exists a unique solution* $(\vec{u}, X(t))$ *to* (3.24) *complemented by the ODE for the interface* (3.26) *subject to nonlinear boundary conditions given by* (3.25)*.*

Nevertheless, one of our boundary conditions, specifically our energy boundary condition from (3.23), is nonlinear.

Proof. We sought to address this issue by making the following change of variables described in Assumption 6.7(iii) of [2] and adapted to our case

$$\vec{v} = \Theta(\vec{u}) = \begin{pmatrix} \Psi_1(\vec{u}) \\ \Psi_2(\vec{u}) \\ \vec{\theta}(\vec{u})\end{pmatrix} \in \mathbb{R}^4, \tag{4.9}$$

where

$$\Psi_1(\vec{u}) = v_f - v_s, \qquad \Psi_2(\vec{u}) = \frac{1}{2}\rho_f g((h_0+\zeta)^2 - {h_0}^2) + Ew, \tag{4.10}$$

are our two boundary conditions and $\vec{\theta}(\vec{u})$ is a map from $\mathbb{R}^4 \longrightarrow \mathbb{R}^2$ whose existence is guaranteed by the Lopatinsky condition and the inverse function theorem, as $D\vec{\Psi}$ has rank two and consequently $\vec{\theta}(\vec{u})$ can be obtained by completing a construct of a $\mathbb{R}^4$ basis using the two linearly independent row vectors in $D\vec{\Psi}$. Hence our updated system is given by

$$\frac{\partial \vec{v}}{\partial t} + \underline{A}(\vec{v})\frac{\partial \vec{v}}{\partial x} = 0, \tag{4.11}$$

with updated linear boundary conditions

$$\begin{cases} \vec{e}_1 \cdot \vec{v} = 0, \\ \vec{e}_2 \cdot \vec{v} = 0, \end{cases} \tag{4.12}$$

where $\underline{A}(\vec{v})$ is obtained by conjugating $A(\vec{u})$ and $\{\vec{e}_1, \vec{e}_2, \vec{e}_3, \vec{e}_4\}$ is the standard basis of $\mathbb{R}^4$. Now we can properly apply Theorem 3.19 to this updated system with linear boundary conditions and show that a unique solution exists for said system and therefore for (4.7), as change of variables can easily bring us back to the original system.

Now let us take a look at the four assumptions described in Theorem 4.1. To start with, a) is clear in our scenario as the matrices $A_{L,R}$ and the scalar function χ are polynomial in ζ, v_f, w, v_s. Then, since $\underline{A}(\vec{v})$ is similar to $A(\vec{u})$, they share the same eigenvalues and hence the condition on strict hyperbolicity transfers over; as a result, we could just show that the original system is strictly hyperbolic. Solving the characteristic polynomials $\det(D\mathcal{F}_f - \lambda_L \mathbb{I}) = 0$ and $\det(D\mathcal{F}_s - \lambda_R \mathbb{I}) = 0$ yields the eigenvalues on the fluid and solid side

$$\lambda_L = v_f \pm \sqrt{gh}, \qquad \lambda_R = \pm\sqrt{\frac{E}{\rho_s}}. \tag{4.13}$$

Since both E and ρ_s are greater than zero, the eigenvalues on the solid side are real and simple, and as long as $\zeta > -h_0$, the eigenvalues on the fluid side are real. Therefore, the Saint-Venant equations are strictly hyperbolic on $U = \{(\zeta, v_f) : \zeta > -h_0\}$ and the wave equations are unconditionally strictly hyperbolic.

Now as for the invertibility of the Kreiss-Lopatinsky matrix, let us first discuss the case with the original coupled system. By Equation 3.8 of [2], the Lopatinsky matrix in our scenario is given by

$$L_{2\times 2}(\vec{u}) = D\vec{\Psi}(\vec{u}) \begin{pmatrix} \vec{v_L^-} & 0_{2\times 1} \\ 0_{2\times 1} & \vec{v_R^+} \end{pmatrix}, \tag{4.14}$$

where $\vec{\Psi} : \mathbb{R}^4 \longrightarrow \mathbb{R}^2$ is the vector-valued function corresponding to the boundary conditions, $D\vec{\Psi}$ is the corresponding Jacobian matrix, c_0 is some strictly-positive constant to be determined, and $\vec{v_L^-}$, $\vec{v_R^+}$ correspond to the in-going and out-going eigenvectors of the matrix $D\mathcal{F}_f$ and $D\mathcal{F}_s$, respectively, or

$$\vec{v_L^-} = \begin{pmatrix} -\sqrt{h} \\ \sqrt{g} \end{pmatrix}, \qquad \vec{v_R^+} = \begin{pmatrix} -\sqrt{\rho_s} \\ \sqrt{E} \end{pmatrix}.$$

Hence our Lopatinsky condition is as follows:

$$\left| \det\left(D\vec{\Psi}(\zeta, v_f, w, v_s) \begin{pmatrix} \vec{v_L^-} & 0_{2\times 1} \\ 0_{2\times 1} & \vec{v_R^+} \end{pmatrix} \right) \right| \geq c_0. \tag{4.15}$$

Writing out the Jacobian matrix yields

$$D\vec{\Psi}(\zeta, v_f, w, v_s) = \begin{pmatrix} \dfrac{\partial \Psi_1}{\partial \zeta} & \dfrac{\partial \Psi_1}{\partial v_f} & \dfrac{\partial \Psi_1}{\partial w} & \dfrac{\partial \Psi_1}{\partial v_s} \\ \dfrac{\partial \Psi_2}{\partial \zeta} & \dfrac{\partial \Psi_2}{\partial v_f} & \dfrac{\partial \Psi_2}{\partial w} & \dfrac{\partial \Psi_2}{\partial v_s} \end{pmatrix} = \begin{pmatrix} 0 & 1 & 0 & -1 \\ \rho_f g(h_0+\zeta) & 0 & E & 0 \end{pmatrix},$$

and consequently the Lopatinsky determinant becomes

$$\left| \det \left(\begin{pmatrix} 0 & 1 & 0 & -1 \\ \rho_f g(h_0+\zeta) & 0 & E & 0 \end{pmatrix} \begin{pmatrix} -\sqrt{h} & 0 \\ \sqrt{g} & 0 \\ 0 & -\sqrt{\rho_s} \\ 0 & \sqrt{E} \end{pmatrix} \right) \right|.$$

Multiplying the matrices out gives us

$$\left| \det \begin{pmatrix} \sqrt{g} & -\sqrt{E} \\ -\rho_f g(h_0+\zeta)^{\frac{3}{2}} & -E\sqrt{\rho_s} \end{pmatrix} \right|,$$

and therefore we have

$$\left| \rho_f g(h_0+\zeta)^{\frac{3}{2}} + \sqrt{\rho_s g E} \right| \geq c_0. \tag{4.16}$$

Choosing

$$|\zeta| \leq \frac{1}{2} h_0, \tag{4.17}$$

ensures that (4.16) holds for some $c_0 > 0$ and that the corresponding Lopatinsky determinant is uniformly bounded from below for all v_f, v_s, w. Fortunately, the Lopatinsky condition carries over as well, which we will now briefly show. The Lopatinsky matrix of (4.11) is given by

$$L_{2\times 2}(\vec{v}) = D\vec{\Phi}(\vec{v}) \left(\Theta'(\vec{u}) \begin{pmatrix} \vec{v_L^-} \\ 0_{2\times 1} \end{pmatrix} \quad \Theta'(\vec{u}) \begin{pmatrix} 0_{2\times 1} \\ \vec{v_R^+} \end{pmatrix} \right), \tag{4.18}$$

where $\vec{\Phi}(\vec{v}) = \begin{pmatrix} \Phi_1(\vec{v}) \\ \Phi_2(\vec{v}) \end{pmatrix} = \begin{pmatrix} \Psi_1 \\ \Psi_2 \end{pmatrix}$ and $\Theta'(\vec{u}) = D\vec{v}$. Thus

$$D\vec{\Phi}(\Psi_1, \Psi_2, \theta_1, \theta_2) = \begin{pmatrix} \dfrac{\partial \Phi_1}{\partial \Psi_1} & \dfrac{\partial \Phi_1}{\partial \Psi_2} & \dfrac{\partial \Phi_1}{\partial \theta_1} & \dfrac{\partial \Phi_1}{\partial \theta_2} \\ \dfrac{\partial \Phi_2}{\partial \Psi_1} & \dfrac{\partial \Phi_2}{\partial \Psi_2} & \dfrac{\partial \Phi_2}{\partial \theta_1} & \dfrac{\partial \Phi_2}{\partial \theta_2} \end{pmatrix} = \begin{pmatrix} 1 & 0 & 0 & 0 \\ 0 & 1 & 0 & 0 \end{pmatrix},$$

and our Lopatinsky condition becomes

$$\left| \det \left(\begin{pmatrix} 1 & 0 & 0 & 0 \\ 0 & 1 & 0 & 0 \end{pmatrix} \begin{pmatrix} \sqrt{g} & -\sqrt{E} \\ -\rho_f g(h_0+\zeta)^{\frac{3}{2}} & -E\sqrt{\rho_s} \\ -\sqrt{h}\frac{\partial \theta_1}{\partial \zeta} + \sqrt{g}\frac{\partial \theta_1}{\partial v_f} & -\sqrt{\rho_s}\frac{\partial \theta_1}{\partial w} + \sqrt{E}\frac{\partial \theta_1}{\partial v_s} \\ -\sqrt{h}\frac{\partial \theta_2}{\partial \zeta} + \sqrt{g}\frac{\partial \theta_2}{\partial v_f} & -\sqrt{\rho_s}\frac{\partial \theta_2}{\partial w} + \sqrt{E}\frac{\partial \theta_2}{\partial v_s} \end{pmatrix} \right) \right| \geq c_0.$$

Simplifying again yields (4.16), which brings us back to the conclusion of (4.17). Since criteria c) from Theorem 3.19 is readily satisfied by restricting ζ, v_f, w, v_s to a sufficiently small set, all three criteria are accounted for and we know that solution exists for the system with linear boundary conditions after change of variables, and subsequently for the original nonlinear hyperbolic system as well. □

5 Linear Stability Analysis

5.1 Linearization

To begin with, we perform linear approximation on the four parameters:

$$\begin{pmatrix} \zeta \\ v_f \\ w \\ v_s \end{pmatrix} = \begin{pmatrix} \underline{\zeta} \\ \underline{v_f} \\ \underline{w} \\ \underline{v_s} \end{pmatrix} + \begin{pmatrix} Z \\ V_f \\ W \\ V_s \end{pmatrix}, \tag{5.1}$$

where $\underline{\zeta}$, $\underline{v_f}$, $\underline{w}$, $\underline{v_s}$ are equilibrium-state constants and Z, V_f, W, V_s are sufficiently small, and thus (4.7) becomes

$$\begin{cases} \dfrac{\partial}{\partial t}\begin{pmatrix} Z \\ V_f \end{pmatrix} = -\begin{pmatrix} \underline{v_f} & h_0 + \underline{\zeta} \\ g & \underline{v_f} \end{pmatrix} \dfrac{\partial}{\partial x}\begin{pmatrix} Z \\ V_f \end{pmatrix}, & x < X(t), \\ \dfrac{\partial}{\partial t}\begin{pmatrix} W \\ V_s \end{pmatrix} = \begin{pmatrix} 0 & 1 \\ \frac{E}{\rho_s} & 0 \end{pmatrix} \dfrac{\partial}{\partial x}\begin{pmatrix} W \\ V_s \end{pmatrix}, & x > X(t). \end{cases} \tag{5.2}$$

Now for all functions $T(x,t)$ where $T \in \{Z, V_f, W, V_s\}$, we make the following transformation

$$T(x,t) \longrightarrow T(x - X(t), t), \tag{5.3}$$

and thus

$$\begin{aligned} \frac{\partial T(x,t)}{\partial t} &= -X'(t)\frac{\partial T}{\partial x} + \frac{\partial T}{\partial t}, \\ \frac{\partial T(x,t)}{\partial x} &= \frac{\partial T}{\partial x}. \end{aligned} \tag{5.4}$$

Plugging (5.4) into (5.2) gives

$$\begin{cases} \dfrac{\partial}{\partial t}\begin{pmatrix} Z \\ V_f \end{pmatrix} = -\begin{pmatrix} V_f + X'(t) & h_0 + \underline{\zeta} \\ g & V_f + X'(t) \end{pmatrix} \dfrac{\partial}{\partial x}\begin{pmatrix} Z \\ V_f \end{pmatrix}, & x < 0, \\ \dfrac{\partial}{\partial t}\begin{pmatrix} W \\ V_s \end{pmatrix} = \begin{pmatrix} X'(t) & 1 \\ \frac{E}{\rho_s} & X'(t) \end{pmatrix} \dfrac{\partial}{\partial x}\begin{pmatrix} W \\ V_s \end{pmatrix}, & x > 0, \end{cases} \tag{5.5}$$

Observe that now the discontinuity occurs at the fixed coordinates $x = 0$ instead of $X(t)$. Now we would like to linearize the boundary conditions as well. First, just like those four variables in (5.1), we approximate the contact line as

$$X(t) = \underline{v_f} t + Y(t), \tag{5.6}$$

and thus differentiating would give us the kinematic boundary condition. Together with the approximations from (5.1) and boundary conditions from (3.11) and (3.23), our linearized boundary conditions are given by

$$\begin{cases} V_f = V_s, & x = 0, \\ \rho_f g(h_0 + \underline{\zeta})Z + EW = 0, & x = 0, \end{cases} \tag{5.7}$$

Now for simplicity sake, we set

$$\begin{pmatrix} \underline{\zeta} \\ \underline{v_f} \\ \underline{w} \\ \underline{v_s} \end{pmatrix} = \vec{0}.$$

First, note that this would turn (5.6) into just $X(t) = Y(t)$, and thus from now on to avoid adding a new variable, we will keep using $X(t)$ in the linearized setting. More importantly, our fully-linearized coupled system becomes

$$\begin{cases} \dfrac{\partial}{\partial t}\begin{pmatrix} Z \\ V_f \end{pmatrix} = -\begin{pmatrix} 0 & h_0 \\ g & 0 \end{pmatrix}\dfrac{\partial}{\partial x}\begin{pmatrix} Z \\ V_f \end{pmatrix}, & x < 0, \\ \dfrac{\partial}{\partial t}\begin{pmatrix} W \\ V_s \end{pmatrix} = \begin{pmatrix} 0 & 1 \\ \frac{E}{\rho_s} & 0 \end{pmatrix}\dfrac{\partial}{\partial x}\begin{pmatrix} W \\ V_s \end{pmatrix}, & x > 0, \\ V_f = V_s, & x = 0, \\ \rho_f g h_0 Z + EW = 0, & x = 0, \\ X'(t) = V_f, & x = 0. \end{cases} \tag{5.8}$$

It is worth noting that $X'(t)$ is also small and so can be dropped from the matrices; in the actual problem $X'(t)$ is nonzero. For (5.8), we propose the following solution form

$$T(x,t) = e^{\lambda t}\hat{T}(x), \tag{5.9}$$

where $\lambda \in \mathbb{C}$ and $T \in \{Z, V_f, W, V_s\}$, and the boundary $X(t)$, $X'(t)$ takes the form

$$X(t) = e^{\lambda t}\hat{X}(\lambda), \tag{5.10}$$

where $\hat{X}(\lambda)$ is some constant depending on λ, and thus

$$X'(t) = \lambda e^{\lambda t}\hat{X}(\lambda) = e^{\lambda t}\hat{v_{f1}}(0).$$

Plugging (5.9) and (5.10) into (5.8) gives us

$$\begin{cases} \lambda\begin{pmatrix} \hat{Z}(x) \\ \hat{V}_f(x) \end{pmatrix} = -\begin{pmatrix} 0 & h_0 \\ g & 0 \end{pmatrix}\dfrac{d}{dx}\begin{pmatrix} \hat{Z}(x) \\ \hat{V}_f(x) \end{pmatrix}, & x < 0, \\ \lambda\begin{pmatrix} \hat{W}(x) \\ \hat{V}_s(x) \end{pmatrix} = \begin{pmatrix} 0 & 1 \\ \frac{E}{\rho_s} & 0 \end{pmatrix}\dfrac{d}{dx}\begin{pmatrix} \hat{W}(x) \\ \hat{V}_s(x) \end{pmatrix}, & x > 0, \\ \hat{V}_f(x) = \hat{V}_s(x), & x = 0, \\ \rho_f g h_0 \hat{Z}(x) + E\hat{W}(x) = 0, & x = 0, \\ \lambda\hat{X}(\lambda) = \hat{V}_f(x), & x = 0. \end{cases} \tag{5.11}$$

Let

$$P = \begin{pmatrix} 0 & h_0 \\ g & 0 \end{pmatrix}, \qquad Q = \begin{pmatrix} 0 & 1 \\ \frac{E}{\rho_s} & 0 \end{pmatrix},$$

where matrix P and Q are nonsingular. Now we can write the first two equations in (5.11) as a system of standard first-order ODE with respect to vector-valued functions

$$\begin{aligned} \frac{d\vec{p}}{dx} &= -\lambda P^{-1}\vec{p}, \qquad && x < 0, \\ \frac{d\vec{q}}{dx} &= \lambda Q^{-1}\vec{q}, && x > 0. \end{aligned} \tag{5.12}$$

where

$$\vec{p} = \begin{pmatrix} \hat{Z}(x) \\ \hat{V}_f(x) \end{pmatrix}, \qquad \vec{q} = \begin{pmatrix} \hat{W}(x) \\ \hat{V}_s(x) \end{pmatrix}.$$

5.2 Lax-Majda Analysis

Now we can find the eigenvalues λ_p of $-\lambda P^{-1}$ by setting $\det(-\lambda P^{-1} - \lambda_p \mathbb{I}) = 0$. Solving the corresponding characteristic polynomial gives us

$$\lambda_p^+ = \frac{\lambda}{\sqrt{gh_0}}, \qquad \lambda_p^- = -\frac{\lambda}{\sqrt{gh_0}}. \tag{5.13}$$

with corresponding eigenvectors

$$\vec{v_p^+} = \begin{pmatrix} -h_0 \\ \sqrt{gh_0} \end{pmatrix}, \qquad \vec{v_p^-} = \begin{pmatrix} h_0 \\ \sqrt{gh_0} \end{pmatrix}. \tag{5.14}$$

Similarly, we can find the eigenvalues λ_q of λQ^{-1}

$$\lambda_q^+ = \lambda\sqrt{\frac{\rho_s}{E}}, \qquad \lambda_q^- = -\lambda\sqrt{\frac{\rho_s}{E}}, \tag{5.15}$$

with corresponding eigenvectors

$$\vec{v_q^+} = \begin{pmatrix} 1 \\ \sqrt{\frac{E}{\rho_s}} \end{pmatrix}, \qquad \vec{v_q^-} = \begin{pmatrix} -1 \\ \sqrt{\frac{E}{\rho_s}} \end{pmatrix}. \tag{5.16}$$

Thus the solution to (5.12) has the form

$$\begin{cases} \vec{p}(x) = c_{p1}e^{\lambda_p^+ x}\vec{v_p^+} + c_{p2}e^{\lambda_p^- x}\vec{v_p^-}, & x < 0, \\ \vec{q}(x) = c_{q1}e^{\lambda_q^+ x}\vec{v_q^+} + c_{q2}e^{\lambda_q^- x}\vec{v_q^-}, & x > 0, \end{cases} \tag{5.17}$$

where c_{p1}, c_{p2}, c_{q1}, c_{q2} are some known constants (specifically, they are the entries of the vectors $P^{-1}\begin{pmatrix} \hat{Z}(0) \\ \hat{V}_f(0) \end{pmatrix}$, $Q^{-1}\begin{pmatrix} \hat{W}(0) \\ \hat{V}_s(0) \end{pmatrix}$). Now in order to determine linear stability, we consider cases based on the sign of the real part of λ. First, let us consider when $\mathrm{Re}(\lambda) \neq 0$. In this case, we want $\vec{p}$ and $\vec{q}$ to decay as $x \to \pm\infty$. If $\mathrm{Re}(\lambda) > 0$, we discard

the eigenvalues λ_p^- and λ_q^+ as we are looking for eigenvectors which decay in x, and that leaves us

$$\begin{cases} \vec{p} = \begin{pmatrix} \hat{Z}(x) \\ \hat{V}_f(x) \end{pmatrix} = c_{p1} \exp\left(\frac{\lambda}{\sqrt{gh_0}} x \right) \begin{pmatrix} -h_0 \\ \sqrt{gh_0} \end{pmatrix}, & x < 0, \\ \vec{q} = \begin{pmatrix} \hat{W}(x) \\ \hat{V}_s(x) \end{pmatrix} = c_{q2} \exp\left(-\lambda \sqrt{\frac{\rho_s}{E}} x \right) \begin{pmatrix} -1 \\ \sqrt{\frac{E}{\rho_s}} \end{pmatrix}, & x > 0, \end{cases} \tag{5.18}$$

and from (5.11) we have the boundary conditions

$$\begin{cases} \hat{V}_f(x) = \hat{V}_s(x), & x = 0, \\ \rho_f g h_0 \hat{Z}(x) + E\hat{W}(x) = 0, & x = 0, \\ \lambda \hat{X}(\lambda) = \hat{V}_f(x), & x = 0. \end{cases}$$

If we plug (5.18) into the above, we get

$$\begin{cases} \sqrt{gh_0} c_{p1} - \sqrt{\frac{E}{\rho_s}} c_{q2} = 0, \\ \rho_f g {h_0}^2 c_{p1} + E c_{q2} = 0, \\ X'(t) = \sqrt{gh_0} c_{p1}. \end{cases} \tag{5.19}$$

Conversely if $\mathrm{Re}(\lambda) < 0$, we discard the eigenvalues λ_p^+ and λ_q^-, which leaves us

$$\begin{cases} \vec{p} = \begin{pmatrix} \hat{Z}(x) \\ \hat{V}_f(x) \end{pmatrix} = c_{p2} \exp\left(-\frac{\lambda}{\sqrt{gh_0}} x \right) \begin{pmatrix} h_0 \\ \sqrt{gh_0} \end{pmatrix}, & x < 0, \\ \vec{q} = \begin{pmatrix} \hat{W}(x) \\ \hat{V}_s(x) \end{pmatrix} = c_{q1} \exp\left(\lambda \sqrt{\frac{\rho_s}{E}} x \right) \begin{pmatrix} 1 \\ \sqrt{\frac{E}{\rho_s}} \end{pmatrix}, & x > 0, \end{cases} \tag{5.20}$$

and plugging in (5.20) into (5.11) gives us

$$\begin{cases} \sqrt{gh_0} c_{p2} - \sqrt{\frac{E}{\rho_s}} c_{q1} = 0, \\ \rho_f g {h_0}^2 c_{p2} + E c_{q1} = 0, \\ X'(t) = \sqrt{gh_0} c_{p2}. \end{cases} \tag{5.21}$$

Notice that the matrix corresponding to (5.19) and (5.21)

$$R = \begin{pmatrix} \sqrt{gh_0} & -\sqrt{\frac{E}{\rho_s}} & 0 \\ \rho_f g {h_0}^2 & E & 0 \\ \sqrt{gh_0} & 0 & -1 \end{pmatrix}$$

is nonsingular. Therefore the only solution to (5.19) and (5.21) is

$$\begin{pmatrix} c_{p1} \\ c_{q2} \\ X'(t) \end{pmatrix} = \begin{pmatrix} c_{p2} \\ c_{q1} \\ X'(t) \end{pmatrix} = \vec{0} \in N(R). \tag{5.22}$$

In other words, there are no decaying eigenfunctions when $\mathrm{Re}(\lambda) \neq 0$.

Remark 5.1. *As a result, there is no decay in time due to conservation of energy, or as we can see from the boundary conditions, they leave no freedom for the coefficients other than being zero. Also, it is important to note that this zero background state is at the bottom of a potential energy well, and thus it is stable.*

Now let's consider the scenario when $\mathrm{Re}(\lambda) = 0$, in which case the solutions are purely oscillatory and we can rewrite λ as

$$\lambda = i\omega,$$

where ω is the angular frequency. Since there is no decay, we'd like to keep all of our eigenvalues and thus our solution becomes

$$\begin{cases} \vec{p} = c_{p1} \exp\left(\dfrac{i\omega}{\sqrt{gh_0}}\, x\right) \begin{pmatrix} -h_0 \\ \sqrt{gh_0} \end{pmatrix} + c_{p2} \exp\left(-\dfrac{i\omega}{\sqrt{gh_0}}\, x\right) \begin{pmatrix} h_0 \\ \sqrt{gh_0} \end{pmatrix}, & x < 0, \\ \vec{q} = c_{q1} \exp\left(i\omega \sqrt{\dfrac{\rho_s}{E}}\, x\right) \begin{pmatrix} 1 \\ \sqrt{\frac{E}{\rho_s}} \end{pmatrix} + c_{q2} \exp\left(-i\omega \sqrt{\dfrac{\rho_s}{E}}\, x\right) \begin{pmatrix} -1 \\ \sqrt{\frac{E}{\rho_s}} \end{pmatrix}, & x > 0, \end{cases} \tag{5.23}$$

and thus along with the solution form in (5.9), we write

$$\begin{aligned} \begin{pmatrix} Z \\ V_f \end{pmatrix} &= e^{i\omega t} \vec{p} \\ &= c_{p1} \exp\left(\frac{i\omega}{\sqrt{gh_0}}(x + \sqrt{gh_0}t)\right) \begin{pmatrix} -h_0 \\ \sqrt{gh_0} \end{pmatrix} \\ &\quad + c_{p2} \exp\left(-\frac{i\omega}{\sqrt{gh_0}}(x - \sqrt{gh_0}t)\right) \begin{pmatrix} h_0 \\ \sqrt{gh_0} \end{pmatrix}, \\ \begin{pmatrix} W \\ V_s \end{pmatrix} &= e^{i\omega t} \vec{q} \\ &= c_{q1} \exp\left(i\omega \sqrt{\frac{\rho_s}{E}} \left(x + \sqrt{\frac{E}{\rho_s}} t\right)\right) \begin{pmatrix} 1 \\ \sqrt{\frac{E}{\rho_s}} \end{pmatrix} \\ &\quad + c_{q2} \exp\left(-i\omega \sqrt{\frac{\rho_s}{E}} \left(x - \sqrt{\frac{E}{\rho_s}} t\right)\right) \begin{pmatrix} -1 \\ \sqrt{\frac{E}{\rho_s}} \end{pmatrix}. \end{aligned} \tag{5.24}$$

(5.24) basically tell us when there is no decay, both the fluid and the solid consist of waves travelling in opposite directions, collectively obeying the local conservation of energy for plane waves. Speaking of which, let's plug the solution from (5.23) into the energy boundary conditions in (5.11) with the added constraint on $X'(t)$, and that yields

$$\begin{cases} \sqrt{gh_0}(c_{p1} + c_{p2}) - \sqrt{\frac{E}{\rho_s}}(c_{q1} + c_{q2}) = 0, \\ \rho_f g {h_0}^2 (c_{p1} - c_{p2}) + E(c_{q1} - c_{q2}) = 0, \\ X'(t) = \sqrt{gh_0}(c_{p1} + c_{p2}), \end{cases} \tag{5.25}$$

and we can write the solution form to the above as

$$\vec{c}(t) = \begin{pmatrix} c_{p1} \\ c_{p2} \\ c_{q1} \\ c_{q2} \\ X'(t) \end{pmatrix} = \mathrm{span}\left(\begin{pmatrix} \frac{E}{\rho_f g {h_0}^2} \\ -\frac{E}{\rho_f g {h_0}^2} \\ -1 \\ 1 \\ 0 \end{pmatrix}, \begin{pmatrix} \frac{1}{2\sqrt{gh_0}} - \frac{E\sqrt{\rho_s E}}{2\rho_f g {h_0}^2} \\ \frac{1}{2\sqrt{gh_0}} + \frac{E\sqrt{\rho_s E}}{2\rho_f g {h_0}^2} \\ \sqrt{\frac{\rho_s}{E}} \\ 0 \\ 1 \end{pmatrix} \right) = N(R'), \tag{5.26}$$

where

$$R' = \begin{pmatrix} \sqrt{gh_0} & \sqrt{gh_0} & -\sqrt{\frac{E}{\rho_s}} & -\sqrt{\frac{E}{\rho_s}} & 0 \\ \rho_f g{h_0}^2 & -\rho_f g{h_0}^2 & E & -E & 0 \\ \sqrt{gh_0} & \sqrt{gh_0} & 0 & 0 & -1 \end{pmatrix}.$$

Therefore, solutions certainly exist for (5.11) in pure oscillatory forms when $\mathrm{Re}(\lambda) = 0$.

5.3 Transmission & Reflection Coefficients

Now we wish to find the transmittance coefficient c_T and reflection coefficient c_R of the fluid travelling wave through the boundary. First we set the corresponding rightward fluid traveling wave coefficient and leftward solid traveling wave coefficient to one and zero, respectively, or

$$c_{p2} = 1, \qquad c_{q1} = 0,$$

so that our focus is purely on the waves transmitted and reflected. Thus, from (5.24) we write

$$\begin{cases} Z = h_0 \left(e^{-\frac{i\omega}{\sqrt{gh_0}}(x-\sqrt{gh_0}t)} - c_R e^{\frac{i\omega}{\sqrt{gh_0}}(x+\sqrt{gh_0}t)} \right), \\ V_f = \sqrt{gh_0} \left(e^{-\frac{i\omega}{\sqrt{gh_0}}(x-\sqrt{gh_0}t)} + c_R e^{\frac{i\omega}{\sqrt{gh_0}}(x+\sqrt{gh_0}t)} \right), \\ W = -c_T e^{-i\omega\sqrt{\frac{\rho_s}{E}}(x-\sqrt{\frac{E}{\rho_s}}t)}, \\ V_s = c_T \sqrt{\frac{E}{\rho_s}} e^{-i\omega\sqrt{\frac{\rho_s}{E}}(x-\sqrt{\frac{E}{\rho_s}}t)}, \end{cases} \tag{5.27}$$

and plugging (5.27) into the linearized boundary conditions from (5.8) gives us the following linear system

$$\begin{cases} \sqrt{gh_0}(1 + c_R) - \sqrt{\frac{E}{\rho_s}} c_T = 0, \\ \rho_f g{h_0}^2 (1 - c_R) - E c_T = 0. \end{cases} \tag{5.28}$$

Solving the above system yields

$$\begin{cases} c_R = \dfrac{\rho_f g{h_0}^2 - \sqrt{\rho_s E g h_0}}{\rho_f g{h_0}^2 + \sqrt{\rho_s E g h_0}}, \\ \\ c_T = \dfrac{2\rho_f g{h_0}^2 \sqrt{\rho_s h_0}}{\rho_f {h_0}^2 \sqrt{gE} + E\sqrt{\rho_s h_0}}. \end{cases} \tag{5.29}$$

Observe that c_R is strictly less than one while c_T doesn't have to be. In case of a decrease in acoustic impedance, the c_T can be greater than one, but in our scenario we can safely assume that both c_R and c_T are less than one.

5.4 Energy Balance

We'd now like to take a closer look at the energy balance to the original nonlinear system in bounded domains. Recall that from (3.12) the change in fluid energy density can be written as

$$\mathcal{E}_f'(t) = \int_{-\infty}^{X(t)} \frac{\partial e_f}{\partial t}\, dx + X'(t) e_f(X(t), t), \tag{5.30}$$

and thus for the fixed fluid boundary $x = -L$, where $-L$ is the leftward boundary for the fluid, $\mathcal{E}_f'(t)$ becomes

$$\mathcal{E}_f'(t) = -\mathcal{F}_f\Big|_{-L}^{X(t)} + X'(t)e_f(X(t),t). \tag{5.31}$$

Here, we'd like to solely focus on the energy change at the incoming mode on the fluid side at $x = -L$ as the coupling problem at the boundary is taken care of by the energy boundary conditions discussed in the modeling section. Thus we write

$$\begin{aligned}\mathcal{E}_f'(t)\big|_{-L} &= -\Pi h v_f\big|_{-L}, \\ &= (h_0 + \zeta(-L,t))v_f(-L,t)\left(\frac{1}{2}\rho_f {v_f}^2(-L,t) + \rho_f g\zeta(-L,t)\right).\end{aligned} \tag{5.32}$$

Now as for ζ and v_f, note that we need the general solution to the linearized Saint-Venant equations linearized about $\begin{pmatrix}\zeta \\ v_f\end{pmatrix} = \vec{0}$, which is given by

$$\begin{pmatrix}\zeta \\ v_f\end{pmatrix} = f(x - \sqrt{gh_0}t)\begin{pmatrix}h_0 \\ \sqrt{gh_0}\end{pmatrix} + g(x + \sqrt{gh_0}t)\begin{pmatrix}-h_0 \\ \sqrt{gh_0}\end{pmatrix}, \tag{5.33}$$

for arbitrary functions f and g (the pure-oscillatory traveling wave solutions from (5.24) is one example). Let us now take a moment to show that why (5.33) is indeed true. Recall the linearized Saint-Venant equations are in the form of

$$\frac{\partial \vec{u}}{\partial t} + A\frac{\partial \vec{u}}{\partial x} = 0, \tag{5.34}$$

where $\vec{u}(x,t) = \begin{pmatrix}Z \\ V_f\end{pmatrix}$ and $A = \begin{pmatrix}0 & h_0 \\ g & 0\end{pmatrix}$. With respect to the basis $\left\{\begin{pmatrix}h_0 \\ \sqrt{gh_0}\end{pmatrix}, \begin{pmatrix}-h_0 \\ \sqrt{gh_0}\end{pmatrix}\right\}$, which is formed by the eigenvector of A, we obtain $\underline{\vec{u}}$ which can be expressed as

$$\underline{\vec{u}} = \begin{pmatrix}\underline{Z} \\ \underline{V_f}\end{pmatrix} = \begin{pmatrix}0 & h_0 \\ g & 0\end{pmatrix}^{-1}\begin{pmatrix}Z \\ V_f\end{pmatrix}.$$

Hence in the new basis (5.34) becomes

$$\frac{\partial \underline{\vec{u}}}{\partial t} + \begin{pmatrix}\sqrt{gh_0} & 0 \\ 0 & -\sqrt{gh_0}\end{pmatrix}\frac{\partial \underline{\vec{u}}}{\partial x} = 0, \tag{5.35}$$

or

$$\begin{cases}\dfrac{\partial \underline{Z}}{\partial t} + \sqrt{gh_0}\dfrac{\partial \underline{Z}}{\partial x} = 0, \\ \dfrac{\partial \underline{V_f}}{\partial t} - \sqrt{gh_0}\dfrac{\partial \underline{V_f}}{\partial x} = 0.\end{cases} \tag{5.36}$$

Now as it is relatively easy to show that for $u(x,t) \in \mathbb{R}$, the general solution to the PDE

$$\frac{\partial u}{\partial t} + v\frac{\partial u}{\partial x} = 0,$$

takes the form $u = f(x - vt)$ for arbitrary function f, we write out the solution to (5.36) as

$$\underline{Z} = f(x - \sqrt{gh_0}t), \qquad \underline{V_f} = f(x + \sqrt{gh_0}t),$$

for arbitrary functions f and g. Therefore, writing out

$$\begin{pmatrix} Z \\ V_f \end{pmatrix} = \begin{pmatrix} \vec{v}_1 & \vec{v}_2 \end{pmatrix} \begin{pmatrix} f(x - \sqrt{gh_0}t) \\ g(x + \sqrt{gh_0}t) \end{pmatrix},$$

completes the proof for (5.33). Moving on, we have

$$\begin{pmatrix} \zeta \\ v_f \end{pmatrix}(-L, t) = c_{p1}(t) \begin{pmatrix} -h_0 \\ \sqrt{gh_0} \end{pmatrix} + c_{p2}(t) \begin{pmatrix} h_0 \\ \sqrt{gh_0} \end{pmatrix},$$

where

$$c_{p1}(t) = f(-L + \sqrt{gh_0}t), \qquad c_{p2}(t) = g(-L - \sqrt{gh_0}t).$$

Now we wish to set $c_{p1}(t) = 0$ because $c_{p1}(t)$ corresponds to the fluid wave travelling into the fluid and we want to limit the energy input on the leftward fluid boundary, and then we treat $c_{p2}(t)$ as some known function of time. Therefore we write

$$\zeta(-L, t) = c_{p2}(t)h_0, \qquad v_f(-L, t) = c_{p2}(t)\sqrt{gh_0},$$

and plugging the above into (5.32) yields the rate of change in energy at the boundary $x = -L$:

$$\mathcal{E}_f'(t)\big|_{-L} = \rho_f g {h_0}^2 \sqrt{gh_0} c_{p2}(t)^2 (1 + c_{p2}(t))(1 + \frac{1}{2}c_{p2}(t)). \tag{5.37}$$

Here, it is important to note that the above is an approximate calculation as we've used the linearized model, while the original problem remains nonlinear.

6 Numerics

For our numerical model, we utilize a classical finite difference method for hyperbolic partial differential equations, MacCormack's method, with specialized techniques to reconcile the domain shifts caused by the moving boundary. Overall, this technique yields the expected quadratic convergence.

While our model is initially on the real line, we assume the domain $x \in [-L, L]$, enabling us to discretize the spatial domain and approximate solutions at these discrete points using standard finite difference techniques.

Remark 6.1. *Restricting x to a finite domain causes the behavior of simulated solutions to deviate from our actual model once perturbations from equilibrium reach the finite domain boundaries. At this point, the boundary condition begins to have an effect on neighboring cells. This effect then propagates throughout the entire discretized domain, leading to large differences from an infinite spatial setting. In practice, we restrict our observation window to the period of time prior to the perturbations from equilibrium reaching the right hand side boundary, $x = L$, to avoid inaccuracies introduced by this phenomenon.*

While not as quickly convergent or compatible with discontinuities as finite volume or ENO/WENO schemes, we selected MacCormack's method as the base of our numerical approach as the simplicity of the scheme enables easy adaptation to handle the moving fluid-solid boundary within our model. Below, MacCormack's is stated generally before being extended to the specifics of fluid-structure interaction problem.

6.1 MacCormack's Method

MacCormack's Method uses the average of forward and backwards differences to approximate the time evolution of variables modeled using hyperbolic partial differential equations in conservative form with second order convergence [6].

We start with a general system of conservation laws

$$\frac{\partial U}{\partial t} + \frac{\partial F(U)}{\partial x} = 0$$

where U is the vector of unknowns and $F(U)$ is the flux vector. The predictor step of MacCormack's method first approximates the time evolution along the spatial grid using the forward difference in place of the spatial derivative. For the i-th spatial grid point, the predictor step approximates the value of U at the next time step from data available at the n-th time step as follows:

$$U_i^p = U_i^n - \frac{\Delta t}{\Delta x}\left(F(U_{i+1}^n) - F(U_i^n)\right)$$

Δt and Δx are the time and spatial steps. Since we use a uniform grid within our numerical implementation for simplicity, these steps remain constant throughout the modeling process. After the predictor step values are calculated throughout the interior of the spatial grid, the corrector step improves upon these approximations by averaging with an approximation calculated with the backward difference of the values from the predictor step:

$$U_i^{n+1} = \frac{1}{2}(U_i^p + U_i^n) - \frac{\Delta t}{2\Delta x}\left(F(U_i^p) - F(U_{i-1}^p)\right)$$

The process of computing predictor and corrector steps along the interior of the spatial grid is then continued for subsequent time steps to gain a more complete picture of the time evolution of variables constrained by hyperbolic conservation laws.

6.2 Separate Fluid and Solid Domains

Both the fluid and solid equations for our model, (3.1) and (3.2), are systems of hyperbolic partial differential equations in conservative form like (6.1). Thus, we can apply MacCormack's Method as described in Section 6.1 for approximation along the interior of both the fluid and solid domains inside of our model.

Next, we discuss the appropriate numerical boundary conditions for each side of the fluid and solid domains in isolation before approaching the problem of coupling the two domains. These boundaries are fictitious in that they do not exist in Theorem 3.7, but must be implemented to reconcile the finite nature of a numerical domain. First handling the non-linear shallow water wave equations on a fixed domain, $x \in [-L, 0]$, we would like for mass to remain within the boundaries which yields a kinematic boundary condition, $v_f(-L, t) = v_f(0, t) = 0$. From the kinematic boundary condition and (3.1), we see that ζ must have homogeneous Neumann boundary conditions $\frac{\partial \zeta}{\partial x}(-L, t) = \frac{\partial \zeta}{\partial x}(0, t) = 0$. The boundary points at the first spatial index 1, corresponding to $x_1 = -L$, and the last spatial index N, corresponding to $x_N = 0$, are easily handled by setting $(v_f)_1^n = (v_f)_N^n = 0$ satisfying the kinematic boundary condition, while $\zeta_1^n = \zeta_2^n$ and $\zeta_N^n = \zeta_{N-1}^n$ satisfy the Neumann boundary condition for all time indicies n.

The previous method allows us to solve for solutions with no external forcing other than gravity. However, to add external forcing to the fluid system in the form of rightward moving waves, we need to establish new boundary conditions on the left hand side. Recall from the linearized model in (5.14), we are able to approximate the decomposition of ζ and v_f at a given point into leftward and rightward moving components follows,

$$\begin{pmatrix} \zeta \\ v_f \end{pmatrix} = c_{p1} \begin{pmatrix} -h_0 \\ \sqrt{h_0 g} \end{pmatrix} + c_{p2} \begin{pmatrix} h_0 \\ \sqrt{h_0 g} \end{pmatrix}, \tag{6.1}$$

where c_{p1} is the scaling factor for the leftward moving mode. This decomposition provides a linear approximation to the exact split between incoming and outgoing waves. Intuitively, we would like to model incoming rightward moving waves, while leftward moving waves are allowed to exit on the left boundary. This is achieved by a combination of different boundary conditions on the leftward and rightward moving modes at $x = -L$. Specifically, we place inhomogeneous Dirichlet boundary conditions on the rightward moving mode and homogeneous Neumann boundary conditions on the leftward moving mode.

For the numerical implementation, we used a "ghost cell" on the left hand side and a forcing function F which satisfies $F(0) = F'(0) = \cdots = F^{(k)}(0) = 0$ for some $k \geq 1$. The condition on F arises from compatibility constraints with initial conditions of the system. Let the ghost cell be at the first spatial index x_1, corresponding to $x = -L$. After each predictor or corrector step within the MacCormack algorithm, the ghost cell values are

$$\begin{pmatrix} \zeta_1^n \\ (v_f)_1^n \end{pmatrix} = c_{p1} \begin{pmatrix} -h_0 \\ \sqrt{h_0 g} \end{pmatrix} + F(t_n) \begin{pmatrix} h_0 \\ \sqrt{h_0 g} \end{pmatrix}, \tag{6.2}$$

where c_{p1} has the explicit solution based on the adjacent at cell x_2,

$$c_{p1} = \frac{-\zeta_2^n \sqrt{h_0 g} + h_0 (v_f)_2^n}{2 h_0 \sqrt{h_0 g}} \tag{6.3}$$

which follows directly from (6.1). Note that in the MacCormack algorithm, interior values would be calculated first. Then the left ghost cell values are assigned based on the newly found adjacent cell values and the forcing function F.

For linear wave equation solutions on a fixed domain, $x \in [0, L]$, we would again like for mass to remain within the boundaries, so we set kinematic boundary conditions $v_s(0,t) = v_s(L,t) = 0$. The linear wave equations in (3.2) then require Neumann boundary conditions $\frac{\partial w}{\partial x}(0,t) = \frac{\partial w}{\partial x}(L,t) = 0$. For interior points, we once more approximate with the predictor and corrector steps of MacCormack's Method. The boundary conditions are implemented in the same fashion as in the fluid model. Where the first and last spatial indicies are 1 and N, we set $(v_s)_1^n = (v_s)_N^n = 0$, where the spatial index n corresponds to $x = L$ at the right boundary, for the kinematic boundary condition, while $w_1^n = w_2^n$ and $w_N^n = w_{N-1}^n$ for the Neumann boundary condition at all times n.

For the linear wave equation $\frac{\partial^2 u}{\partial t^2} = c^2 \frac{\partial^2 u}{\partial x^2}$ with conditions

$$\begin{aligned} u(0,t) = u(L,t) = 0 \qquad & \text{for all } t, \\ u(x,0) = f(x) \qquad & 0 < x < L, \\ v_s(x,0) = g(x) \qquad & 0 < x < L, \end{aligned}$$

there exists a known analytical solution known as d'Alembert's formula. This analytical solution allows us to check the convergence of the MacCormack implementation. For the

results shown in Figure 1, the values $u(x,0) = \sin(x)$, $v_s(x,0) = 0$, $L = \pi$, $T = 1$ and $c = 1$ were used. For the mesh resolutions, we set $\Delta x = \frac{L}{2^i}$ and $\Delta t = \frac{T}{2^i}$ for $i \in \{4, 5, \ldots, 11\}$. Now defining the ℓ^2 error metric for some numerical solution f^n representing solutions to $f(\cdot, t_n)$, we have

$$\|f^n - f(\cdot, t_n)\|_{\ell^2} = \sqrt{\sum_i (f_i^n - f(x_i, t_n))^2 \Delta x}.$$

At each resolution we calculated the ℓ^2 error of $w(x,T)$ and $v_s(x,t)$ separately and plotted $\log_2\left(\sqrt{\|w^n - w(\cdot,t_n)\|_{\ell^2}^2 + \|v_s^n - v_s(\cdot,t_n)\|_{\ell^2}^2}\right)$ on the y-axis, with the logarithm of the number of x intervals on the x axis.

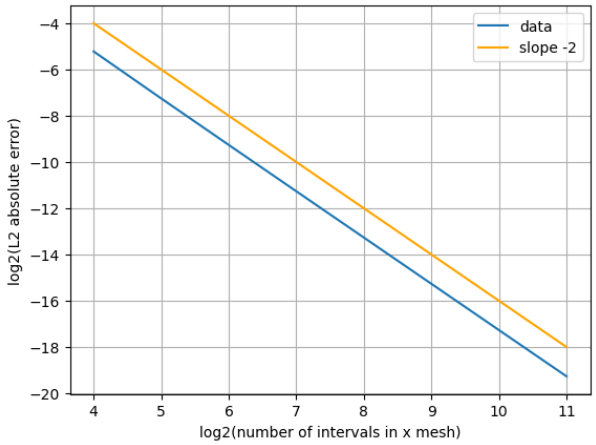

Figure 1: Quadratic convergence of linear wave equation numerical solutions as the spatial and temporal mesh resolutions increase.

The resulting line clearly follows a slope of -2, indicating second-order convergence of w and v_s as expected.

Note that for the non-linear shallow water wave equations, there does not exist an explicit closed form solution. Thus, when calculating the convergence rate for the fixed boundary models above, we used a reference solution which was obtained via the same algorithm with a very high resolution. This reference solution was used as the analytical solution in (6.2), and we saw the expected second order convergence for the fluid models with and without external forcing.

6.3 Fluid and Solid Coupling Method

The full coupled system in our numerical model consists of a spatial and temporal mesh with $x \in [-L, L]$ and $X(0) = 0$. Calculation of all non-boundary points is standard and accomplished via the MacCormack's method steps from 6.2. However, we now have to deal with a moving boundary around the shock located at $X(t)$.

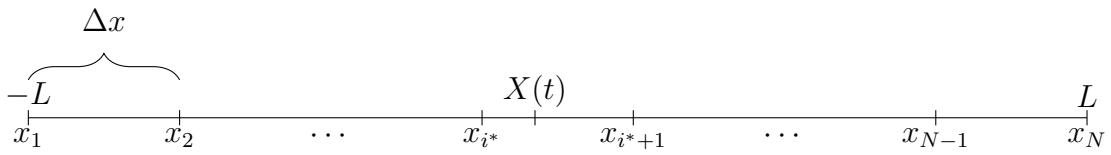

The two shock adjacent cells are x_{i^*} and x_{i^*+1} where $i^* = \lfloor \frac{X(t) - x_1}{\Delta x} \rfloor$. x_{i^*} can be considered the location of the last fluid cell and x_{i^*+1} the location of the first solid cell.

With this setup, there are four boundaries we must consider: the left-hand side boundary of the fluid at $x = -L^+$, the right-hand side boundary of the fluid at $x = X(t)^-$, the left-hand side boundary of the solid at $x = X(t)^+$ and the right-hand side boundary of the solid at $x = L^-$. First addressing the boundary at $x = -L^+$, we use the same condition from (6.2) which has a homogeneous Neumann boundary condition on the leftward moving mode and an inhomogeneous Dirichlet boundary condition on the rightward moving mode with a forcing function $F(t)$. F must satisfy $F(0) = F'(0) = ... = F^{(k)}(0) = 0$ for some $k \geq 1$ which arises from compatibility constraints with initial conditions. The boundary values are set for the cell located at x_1 after each predictor or corrector step within the MacCormack algorithm. This allows us to model incoming waves from the left-hand side.

For the boundary at $x = L$, we use the same boundary conditions as in the solid model in 6.2. Specifically, $v_s(L,t) = 0$ and $\frac{\partial w}{\partial t} = 0$, which is implemented numerically by setting $(v_s)_N^n = 0$ and $w_N^n = w_{N-1}^n$ after each predictor or corrector step.

For the shock adjacent boundaries at $x = X(t)$, some more involved methods are required. Each step of the time-marching process requires finding the new location of $X(t)$. To do this, we first find the velocity of the fluid at the shock boundary at time t_n, denoted as $(v_{fb})^n$, via linear extrapolation

$$(v_{fb})^n = (v_f)_{i^*}^n + \frac{(v_f)_{i^*}^n - (v_f)_{i^*-1}^n}{\Delta x}\left(X(t_n) - x_{i^*}\right) \tag{6.4}$$

and the velocity of the solid at the boundary at time t_n, denoted as $(v_{sb})^n$, by the same method

$$(v_{sb})^n = (v_s)_{i^*+1}^n + \frac{(v_s)_{i^*+2}^n - (v_s)_{i^*+1}^n}{\Delta x}\left(X(t_n) - x_{i^*+1}\right). \tag{6.5}$$

We then take these two extrapolated values and average them to improve the approximation: $X'(t_n) = \frac{1}{2}((v_{fb})^n + (v_{sb})^n)$. By Taylor's Theorem, each of the velocity extrapolations has quadratic error and thus so does the averaged approximation.

We use this to find the next step value by employing the classical two-step Adams-Bashforth method which is second order in time:

$$X(t_{n+1}) = X(t_n) + \Delta t\left(\frac{3}{2}X'(t_n) - \frac{1}{2}X'(t_{n-1})\right). \tag{6.6}$$

The value for $X(t)$ is tracked separately from the spatial mesh. Thus, for our MacCormack method to work, we implement ghost cells surrounding the shock. We place a fluid ghost cell at x_{i^*+1} and a solid ghost cell at x_{i^*}. These locations are outside of the domains of the fluid and solid, so any value corresponding to them, e.g. $\zeta_{i^*+1}^n$ is clearly belonging to a fictitious ghost cell. These ghost cells are key to the coupling method, and their values are derived from the kinematic boundary condition 3.11 and the energy boundary condition 3.23. From these boundary conditions, we derive a formula which converts a solid cell to a fluid cell while preserving boundary conditions,

$$G_{s\to f}\left(\begin{pmatrix} w \\ v_s \end{pmatrix}\right) = \begin{pmatrix} \left(\frac{-2Ew}{\rho_f g} + h_0^2\right)^{1/2} - h_0 \\ v_s \end{pmatrix}, \tag{6.7}$$

and a formula which converts a fluid cell to a solid cell while preserving boundary conditions,

$$G_{f\to s}\left(\begin{pmatrix} \zeta \\ v_f \end{pmatrix}\right) = \begin{pmatrix} \frac{\rho_f g}{2E}\left(\zeta^2 - 2(h_0+\zeta)\zeta\right) \\ v_f \end{pmatrix}, \tag{6.8}$$

where the top entries of both are obtained by solving for either ζ or w in (3.23).

Now we can begin the three step process which is used to generate the ghost cell values. Note that this process is repeated three times: before the predictor step, after the predictor step and after the corrector step. Minor changes are made in each stage, and they will be explained in detail after a demonstration of the process before the predictor step.

First, we start with values for v_f and ζ at locations x_j for $j \in \{1, \ldots, i^*\}$ and values for v_s and w at locations x_k for $k \in \{i^* + 1, \ldots, N\}$. We use linear extrapolation to find values at $x = X(t_n)$,

$$\zeta_b^n = \zeta_{i^*}^n + \frac{\zeta_{i^*}^n - \zeta_{i^*-1}^n}{\Delta x} \left(X(t_n) - x_{i^*} \right), \tag{6.9}$$

$$w_b^n = w_{i^*+1}^n + \frac{w_{i^*+2}^n - w_{i^*+1}^n}{\Delta x} \left(X(t_n) - x_{i^*+1} \right), \tag{6.10}$$

while $(v_{fb})^n$ is obtained from (6.4) and $(v_{sb})^n$ is obtained from (6.5).

Second, we use the ghost cell conversion formulas from (6.7) and (6.8) to create ghost cell boundary values. We denote these ghost cell boundary values with a prefix $\mathcal{G}$ to distinguish them from the values obtained in (6.4), (6.5), (6.9) and (6.10). For the fluid,

$$\begin{pmatrix} \mathcal{G}\zeta_b^n \\ \mathcal{G}(v_{fb})^n \end{pmatrix} = G_{s \to f} \left(\begin{pmatrix} w_b^n \\ (v_{sb})^n \end{pmatrix} \right) \tag{6.11}$$

and for the solid,

$$\begin{pmatrix} \mathcal{G}w_b^n \\ \mathcal{G}(v_{sb})^n \end{pmatrix} = G_{f \to s} \left(\begin{pmatrix} \zeta_b^n \\ (v_{fb})^n \end{pmatrix} \right). \tag{6.12}$$

Third, we generate the shock adjacent ghost cells by linear extrapolation from the boundary with the boundary ghost cells. For the fluid,

$$(v_f)_{i^*+1}^n = \mathcal{G}(v_{fb})^n + \frac{\mathcal{G}(v_{fb})^n - (v_f)_{i^*-1}^n}{X(t_n) - x_{i^*-1}} \left(x_{i^*+1} - X(t_n) \right) \tag{6.13}$$

and

$$\zeta_{i^*+1}^n = \mathcal{G}(\zeta_b)^n + \frac{\mathcal{G}(\zeta_b)^n - \zeta_{i^*-1}^n}{X(t_n) - x_{i^*-1}} \left(x_{i^*+1} - X(t_n) \right). \tag{6.14}$$

For the solid,

$$(v_s)_{i^*}^n = \mathcal{G}(v_{sb})^n + \frac{(v_s)_{i^*+2}^n - \mathcal{G}(v_{sb})^n}{x_{i^*+2} - X(t_n)} \left(x_{i^*} - X(t_n) \right) \tag{6.15}$$

and

$$w_{i^*}^n = \mathcal{G}(w_b)^n + \frac{w_{i^*+2}^n - \mathcal{G}(w_b)^n}{x_{i^*+2} - X(t_n)} \left(x_{i^*} - X(t_n) \right), \tag{6.16}$$

which completes the calculation of shock adjacent ghost cell values before the predictor step. Note that in this step of linear extrapolations, we don't use the known values that are adjacent to the shock. Instead, we use known values from x_{i^*-1} and x_{i^*+2} to avoid numerical issues that may arise from $X(t_n)$ being very close to either x_{i^*} or x_{i^*+1} which could result in division by a very small number.

When calculating shock adjacent ghost cell values after the predictor and corrector steps, the same process is followed with appropriate substitutions. Importantly, $X(t_{n+1})$ from (6.6) is used instead of $X(t_n)$. After the predictor step, predicted values are used instead of values from time t_n. Similarly for the corrector step, corrected values are used instead of values from time t_n.

Once corrected values and ghost cells have been determined, i^* is updated according to $X(t_{n+1})$. Depending on whether or not the updated i^* moves to a different cell, a shock adjacent ghost cell from either the fluid or the solid may become a real cell. If the updated i^* moves by more than one cell, this is indicative of the shock moving at supersonic speed, and the numerical solutions are no longer valid. Additionally, if i^* reaches 1 or N, this is indicative of the shock reaching the edge of the computational window and the solution breaks down.

6.4 Coupled System Results

First we show numerical results for the coupled model using the techniques described in the previous section.

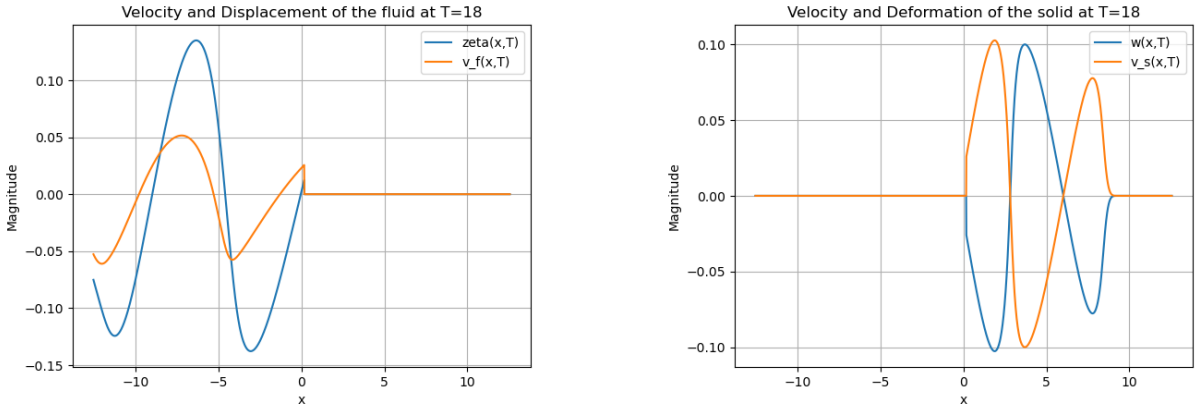

Figure 2: Solution for values $h_0 = 2$, $\rho_f = 1$, $E = 1$, $\rho_s = 1$ and $g = 1$ with forcing function $F(t) = \frac{t^2}{20(1+t^2)} \sin(t)$. The bounds are $L = 4\pi$ and solutions are shown for time $T = 18$.

In the figure above, the system starts at equilibrium and a forcing function introduces waves from the left-hand side which ramp in amplitude. Separate plots are used to show values of ζ and v_f for the fluid on the left and values of w and v_s for the solid on the right. These solutions show the transmission of waves through the shock interface and subtle evidence of wave reflection off of the shock location as seen by the high convexity of v_f at around $x = -4$. The results match our qualitative expectations, although quantitative matching of transmission through the shock remains to be studied quantitatively.

The shift in shock location $X(t)$ is shown more clearly here. As waves first reach the shock location at around time $t = 9$, the solid is compressed, but over time an oscillatory motion begins to appear. These results match our expectations for what might happen as periodic waves interact with an elastic solid.

To test the convergence rate of the algorithm, a reference solution was generated with high resolution via the same methods. The number of spatial steps in the reference was set to 2^{12}, and the number of temporal steps used was 2^{14}. Then we applied a cubic spline interpolation to the reference solution points and used this spline to estimate errors of lower resolution solutions. The left plot in Figure 4 shows $\log_2$ (ℓ^2 absolute error) on the y-axis, which is defined here as the square root of the sum of squares of ℓ^2 norms of w, v_s, ζ and v_s. The right plot in Figure 4 shows $\log_2(X(t)$ error) where $X(t)$ error is the ℓ^2 norm of the error vector with components $\epsilon_i = |X(t_i) - X(t_i)_{ref}|$ for time indicies i at

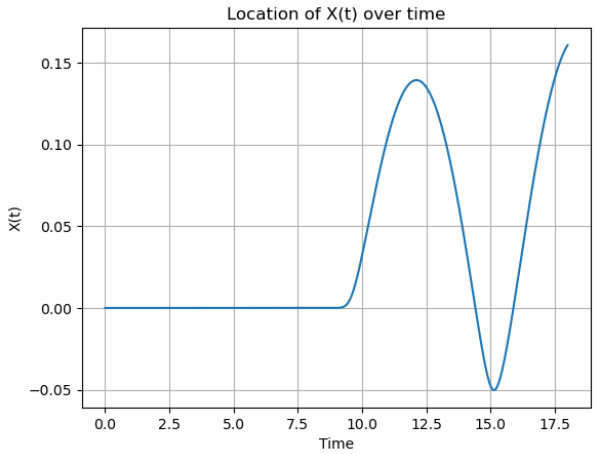

Figure 3: Values of $X(t)$ over time for the same initial conditions and forcing shown in Figure 2.

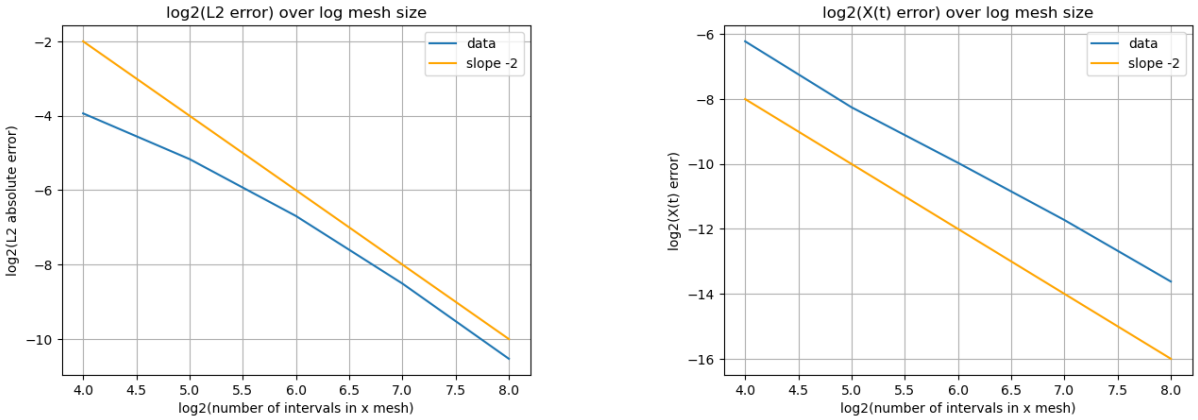

Figure 4: Convergence rate plots for the coupled numerical method. ℓ^2 absolute error is on the left, and $X(t)$ error is on the right.

a given resolution. As seen by the slope of -2 in both plots, the solutions have second order convergence for variables ζ, v_f, w, v_s and the location of the shock $X(t)$.

The two plots above show the convergence of the boundary condition errors as the resolution increases. The boundary velocity error comes from (3.11) and is defined as the max error at any time t_i in the solution, $\max_i |(v_{fb})^i - (v_{sb})^i|$. The energy error is defined similarly as the max energy boundary condition error from (3.23), $\max_i |Ew_b^i + \frac{1}{2}\rho_f g((h_0 + \zeta_b^i)^2 + h_0^2)|$ for any time t_i in the solution. These plots also show slopes of -2 indicating second order convergence for the boundary conditions as well.

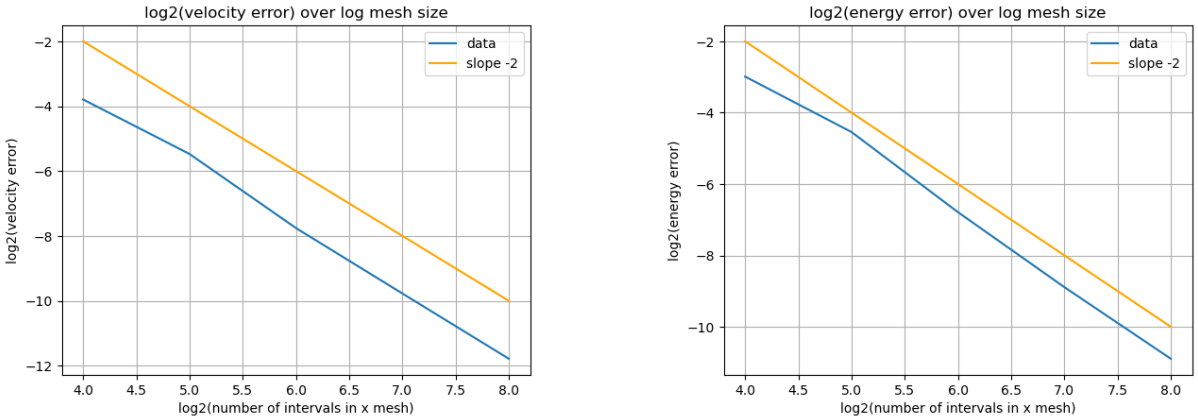

Figure 5: Convergence rate plots for the coupled numerical method. Boundary velocity condition error is on the left, and boundary energy condition error is on the right.

# of x intervals	ℓ^2 abs error	$X(t)$ error	Velocity error	Energy error
16	0.065324	0.013404	0.072170	0.126073
32	0.027885	0.003277	0.022518	0.042921
64	0.009657	0.001001	0.004626	0.009052
128	0.002744	0.000295	0.001142	0.002109
256	0.000676	7.937551e-5	0.000283	0.000525

Table 1: Values from Figures 4 and 5.

References

[1] J. D. Achenbach. *Wave Propagation in Elastic Solids*. North-Holland Publishing Company/American Elsevier, 1973.

[2] T. Iguchi and D. Lannes. Hyperbolic free boundary problems and applications to wave-structure interactions. *Indiana University Mathematics Journal*, 70(1):353–464, 2021.

[3] D. Lannes. *Modeling shallow water waves*. Nonlinearity, 33(5):R1–R57, 2020.

[4] P. D. Lax. Hyperbolic Systems of Conservation Laws II. *Communications on Pure and Applied Mathematics*, 10(4):537–566, 1957.

[5] P. D. Lax. *Hyperbolic systems of conservation laws and the mathematical theory of shock waves*, volume No. 11 of *Conference Board of the Mathematical Sciences Regional Conference Series in Applied Mathematics*. Society for Industrial and Applied Mathematics, Philadelphia, PA, 1973.

[6] R. Maccormack. The effect of viscosity in hypervelocity impact cratering. In *AIAA, Hypervelocity Impact Conference*, number AIAA Paper 69-354. American Inst. of Aeronautics and Astronautics, 1969.

[7] A. Majda. *The Existence of Multi-Dimensional Shock Fronts*. American Mathematical Society: Memoirs of the American Mathematical Society. American Mathematical Society, 1983.

[8] A. Majda. *The Stability of Multi-Dimensional Shock Fronts*. American Mathematical Society: Memoirs of the American Mathematical Society. American Mathematical Society, 1983.

[9] A. Majda. *Compressible Fluid Flow and Systems of Conservation Laws in Several Space Variables*. Applied Mathematical Sciences. Springer New York, 2012.

[10] G. Métivier, T.-P. Liu, J. Smoller, B. Temple, W. Young, K. Zumbrun. *Stability of Multidimensional Shocks*, pages 25–103. 2001.